Electronic Supplementary Material (ESI) for ChemComm.

Electronic Supplementary Information (ESI) for the manuscript:

Magnetocaloric efficiency tuning through solvent-triggered 3D to 2D interconversion in holmium(III)-based dynamic MOFs

N. El Alouani Dahmouni, M. Orts-Arroyo, A. Sanchis-Perucho, N. Moliner, J. Mayans, M. Pacheco, I. Castro,* G. De Munno, N. Marino,* R. Ruiz-García and J. Martínez-Lillo*

Experimental

Materials

Oxalic acid (H_2ox) and holmium(III) nitrate pentahydrate were purchased from commercial sources and used as received.

Synthetic procedures

$\{Ho^{III}_2(ox)_3(H_2O)_6 \cdot xH_2O\}_n$ [x = 4 (1) and 12 (2)]. Aqueous concentrated solutions (0.5 mL) of $Ho(NO_3)_2 \cdot 5H_2O$ (0.220 g, 0.5 mmol) and H_2ox (0.068 g, 0.75 mmol) were placed at the bottom of each of the two arms of an H-shaped tube; water was then added dropwise to completely fill the H-shaped tube which was closed with parafilm. Large plates of **1** or tiny prisms of **2** were obtained after several days or months, respectively, of slow diffusion at 50 °C within a thermostated oven (**1**) or at 5 °C within a refrigerator (**2**). **1**: Yield: 0.135 g (70%). Anal. calcd for $C_6H_{20}Ho_2O_{22}$ (M_w = 774.1 g mol^{-1}): C, 9.31; H, 2.60%. Found: C, 9.45; H, 2.63%. **2**: Yield: 0.149 g (65%). Anal. calcd for $C_6H_{36}Ho_2O_{30}$ (M_w = 918.2 g mol^{-1}): C, 7.85; H, 3.95%. Found: C, 7.75; H, 3.92%. A mixture of large plates of **1** and tiny elongated prisms of **2** suitable for single-crystal X-ray diffraction were obtained after several weeks of slow diffusion at 25 °C.

$[Ho_2(ox)_3]_n$ (3). Crystals of **2** (0.046 g, 0.05 mmol) were placed on a ceramic sample pan; they were then slowly heated and cooled between room temperature and 300 °C under nitrogen atmosphere in a thermobalance to give an amorphous powder of **3**. Yield: 0.030 g (100%). Anal. calcd for $C_6Ho_2O_{12}$ (M_w = 593.9 g mol^{-1}): C, 12.12; H, 0%. Found: C, 12.57; H, 0.01%.

Physical techniques

Elemental analyses (C, H) were performed by the Servei Central de Suport a la Investigació Experimental (SCSIE) de la Universitat de València. Optical microscopy images were taken at 80 amplification by using a Nikon SMZ1000 optical microscope equipped with a Nikon Digital Sight DS-Fi1 camera. The thermogravimetric analysis (TGA) was carried out on powdered samples under a dry N_2 atmosphere (25–550 °C) with a Mettler Toledo TGA/STDA 851 thermobalance operating at a heating rate of 10 °C min^{-1}.

Powder X-ray diffraction (XRD) patterns of powdered samples were collected at room temperature on a D8 Avance A25 Bruker diffractometer by using graphite-monochromated Cu-K_α radiation (λ = 1.54056 Å). The variable-temperature (25–300 °C) powder XRD patterns were collected on a LYNXEYE XE 1-dimensional detector for ultra-fast XRD measurements using an Anton Paar chamber working under a controlled relative humidity of 12%. Measurements were carried out every 5 °C over the angular range 2θ = 8–20°.

Magnetic measurements

Magnetic susceptibility and magnetization measurements were done with a Quantum Design SQUID (Superconducting Quantum Interference Device) magnetometer and a Physical Property Measurement System (PPMS). The magnetic measurements were performed on powdered samples embedded in eicosane to prevent any crystal reorientation. The magnetic data were corrected for the diamagnetism of the constituent atoms and the sample holder.

Crystallographic data collection and refinement

X-ray diffraction data on single crystals of **1** and **2** were collected by means of a Bruker D8 Venture diffractometer with PHOTON II detector using monochromatized Mo-K_α radiation (λ = 0.71073 Å). The structures were solved by standard direct methods and subsequently completed by Fourier recycling by using the SHELXTL software packages. The obtained models were refined with the 2019/3 version of SHELXL against F^2 on all data by full-matrix least squares.[1] All non-hydrogen atoms were refined anisotropically with the aid of rigid bond restraints.[2] **1** contains disordered crystallization water molecules (two per Ho atom). Four different sites have been identified for such molecules, which have been refined with half occupancy each. Also, **2** contains crystallization water molecules (six per Ho atom), only one of which is severely disordered (but notwithstanding was assigned full occupancy in agreement with

[1] Sheldrick, G. M. Crystal structure refinement with SHELXL. *Acta Cryst.*, **2015**, *C71*, 3-8.
[2] Müller, P. Practical suggestions for better crystal structures. *Cryst. Rev.*, **2009**, *15*, 57-83.
[3] A.L.Spek, Acta Cryst. 2009, D65, 148-155.
[4] *CrystalMaker*, CrystalMaker Software, Bicester, England, 2015.
[5] Diamond - Crystal and Molecular Structure Visualization, Crystal Impact - Dr. H. Putz & Dr. K. Brandenburg GbR, Kreuzherrenstr. 102, 53227 Bonn, Germany, https://www.crystalimpact.de/diamond.

thermogravimetric experiments and literature data). The hydrogen atoms on the coordinated water molecules of both **1** and **2** were located on a ΔF map and refined with restrains. Instead, those from the crystallization water molecules were neither found nor calculated. The final calculations were performed with SHELXL and Platon[3], while graphical manipulations were performed with the Crystal Maker[4] and the Diamond programs.[5]

Crystallographic data (excluding structure factors) for the structures reported in this paper have been deposited with the Cambridge Crystallographic Data Centre as supplementary publication numbers CCDC–2351941 (**1**) and CCDC–2351940 (**2**). Copies of the data can be obtained free of charge by application to CCDC, 12 Union Road, Cambridge CB21EZ, UK (fax: (+44) 1223−336−033; e-mail: deposit@ccdc.cam.ac.uk).

Table S1. Summary of crystallographic data for **1** and **2**

	1	**2**
Formula	$C_6H_{20}Ho_2O_{22}$	$C_6H_{36}Ho_2O_{30}$
M (g mol^{-1})	774.1	918.2
Crystal system	Monoclinic	Trigonal
Space group	$P2_1/c$	$R\bar{3}$
a (Å)	10.9347(3)	30.500(9)
b (Å)	9.6040(3)	30.500(9)
c (Å)	9.9542(3)	7.127(2)
α (°)	90	90
β (°)	114.1430(10)	90
γ (°)	90	120
V (Å^3)	953.92(5)	5741(4)
Z	2	9
ρ_{calc} (g cm^{-3})	2.695	2.390
μ (mm^{-1})	8.344	6.281
T (K)	298(2)	297(2)
Reflect. collcd.	14424	6873
Reflect. obs. [$I > 2\sigma(I)$]	2306	2215
Data/Restraints/Parameters	2469/72/173	3241/51/184
R_1[a] [$I > 2\sigma(I)$]	0.0146	0.0642
wR_2[b] [$I > 2\sigma(I)$]	0.0364	0.1393
S[c]	1.115	1.035

[a] $R_1 = \sum(|F_o| - |F_c|)/\sum|F_o|$. [b] $wR_2 = [\sum w(F_o^2 - F_c^2)^2/\sum w(F_o^2)^2]^{1/2}$. [c] $S = [\sum w(|F_o| - |F_c|)^2/(N_o - N_p)]^{1/2}$.

Table S2. Selected bond lengths [Å] and angles [°] for **1**[a]

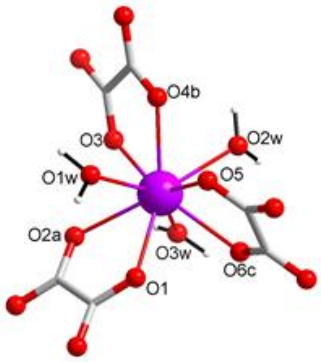

Ho(1) coordination sphere

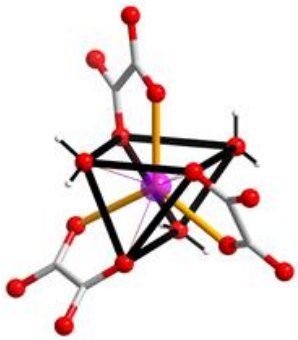

Ho(1) polyhedron viewed as TCTPR

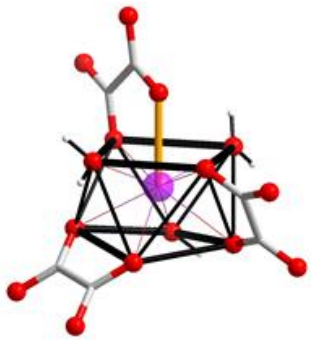

Ho(1) polyhedron viewed as CSAPR

Ho(1)-O(1)	2.4108(19)	Ho(1)-O(4b)	2.4434(19)	Ho(1)-O(1w)	2.376(2)
Ho(1)-O(2a)	2.522(2)	Ho(1)-O(5)	2.3663(18)	Ho(1)-O(2w)	2.430(2)
Ho(1)-O(3)	2.3739(18)	Ho(1)-O(6c)	2.4469(18)	Ho(1)-O(3w)	2.369(2)
O(1)-Ho(1)-O(2a)	65.15(6)	O(2a)-Ho(1)-O(3)	66.03(7)	O(3)-Ho(1)-O(4b)	66.84(6)
O(1)-Ho(1)-O(3)	130.96(7)	O(2a)-Ho(1)-O(4b)	118.08(7)	O(3)-Ho(1)-O(5)	138.29(6)
O(1)-Ho(1)-O(4b)	136.90(7)	O(2a)-Ho(1)-O(5)	140.44(7)	O(3)-Ho(1)-O(6c)	140.55(7)
O(1)-Ho(1)-O(5)	82.12(7)	O(2a)-Ho(1)-O(6c)	116.55(7)	O(3)-Ho(1)-O(1w)	90.03(8)
O(1)-Ho(1)-O(6c)	69.53(7)	O(2a)-Ho(1)-O(1w)	73.53(8)	O(3)-Ho(1)-O(2w)	81.10(7)
O(1)-Ho(1)-O(1w)	72.19(7)	O(2a)-Ho(1)-O(2w)	136.12(8)	O(3)-Ho(1)-O(3w)	73.20(7)
O(1)-Ho(1)-O(2w)	141.54(7)	O(2a)-Ho(1)-O(3w)	69.81(8)		
O(1)-Ho(1)-O(3w)	94.15(8)				
O(4b)-Ho(1)-O(5)	71.47(6)	O(5)-Ho(1)-O(6c)	67.15(6)	O(6c)-Ho(1)-O(1w)	129.25(7)
O(4b)-Ho(1)-O(6c)	125.37(6)	O(5)-Ho(1)-O(1w)	75.79(8)	O(6c)-Ho(1)-O(1w)	72.00(7)
O(4b)-Ho(1)-O(1w)	68.71(7)	O(5)-Ho(1)-O(2w)	83.40(8)	O(6c)-Ho(1)-O(1w)	71.81(7)
O(4b)-Ho(1)-O(2w)	69.24(7)	O(5)-Ho(1)-O(3w)	137.41(7)		
O(4b)-Ho(1)-O(3w)	128.31(8)				
O(1w)-Ho(1)-O(2w)	137.11(8)	O(1w)-Ho(1)-O(3w)	143.27(9)	O(2w)-Ho(1)-O(3w)	73.47(9)

[a]Symmetry codes: (a) -*x*+1, -*y*+1, -*z*+1; (b) -*x*+2, -*y*+1, -*z*+1; (c) -*x*+1, -*y*+1, -*z*.

Table S3. Selected bond lengths [Å] and angles [°] for **2**[a]

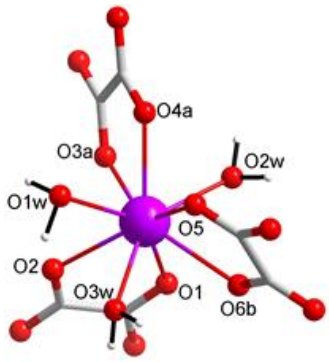

Ho(1) coordination sphere

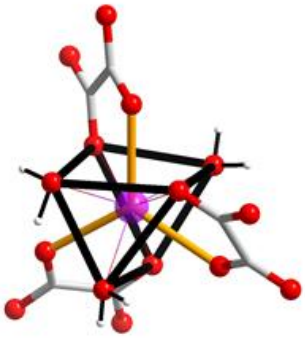

Ho(1) polyhedron viewed as TCTPR

Ho(1) polyhedron viewed as CSAPR

Ho(1)-O(1)	2.354(8)	Ho(1)-O(4a)	2.445(8)	Ho(1)-O(1w)	2.345(9)
Ho(1)-O(2)	2.497(8)	Ho(1)-O(5)	2.416(8)	Ho(1)-O(2w)	2.367(9)
Ho(1)-O(3a)	2.402(8)	Ho(1)-O(6b)	2.513(8)	Ho(1)-O(3w)	2.361(8)
O(1)-Ho(1)-O(2)	66.0(3)	O(2)-Ho(1)-O(3a)	70.1(3)	O(3a)-Ho(1)-O(4a)	66.0(3)
O(1)-Ho(1)-O(3a)	81.1(3)	O(2)-Ho(1)-O(4a)	120.4(3)	O(3a)-Ho(1)-O(5)	135.0(3)
O(1)-Ho(1)-O(4a)	138.3(3)	O(2)-Ho(1)-O(5)	142.5(3)	O(3a)-Ho(1)-O(6b)	137.3(3)
O(1)-Ho(1)-O(5)	133.5(3)	O(2)-Ho(1)-O(6b)	119.2(3)	O(3a)-Ho(1)-O(1w)	88.9(3)
O(1)-Ho(1)-O(6b)	68.5(3)	O(2)-Ho(1)-O(1w)	72.3(3)	O(3a)-Ho(1)-O(2w)	75.2(3)
O(1)-Ho(1)-O(1w)	138.1(3)	O(2)-Ho(1)-O(2w)	130.2(3)	O(3a)-Ho(1)-O(3w)	138.2(3)
O(1)-Ho(1)-O(2w)	74.3(3)	O(2)-Ho(1)-O(3w)	68.8(3)		
O(1)-Ho(1)-O(3w)	88.8(3)				
O(4a)-Ho(1)-O(5)	69.4(3)	O(5)-Ho(1)-O(6b)	65.0(3)	O(6b)-Ho(1)-O(1w)	133.8(3)
O(4a)-Ho(1)-O(6b)	120.3(3)	O(5)-Ho(1)-O(1w)	80.1(3)	O(6b)-Ho(1)-O(1w)	72.2(3)
O(4a)-Ho(1)-O(1w)	68.7(3)	O(5)-Ho(1)-O(2w)	87.0(3)	O(6b)-Ho(1)-O(1w)	68.3(3)
O(4a)-Ho(1)-O(2w)	132.8(3)	O(5)-Ho(1)-O(3w)	79.0(3)		
O(4a)-Ho(1)-O(3w)	73.0(3)				
O(1w)-Ho(1)-O(2w)	141.7(3)	O(1w)-Ho(1)-O(3w)	72.1(3)	O(2w)-Ho(1)-O(3w)	140.4(3)

[a]Symmetry codes: (a) *x*-*y*+2/3, *x*+1/3, -*z*+4/3; (b) -*x*+1, -*y*+1, -*z*+2.

Table S4. Summary of selected structural data for **1** and **2**

	1	**2**
S(TCTPR)[a]	0.672 (1.976)	0.631 (1.561)
S(CSAPR)[a]	0.726 (1.667)	1.151 (2.076)
M–O[b] (Å)	2.471(2)	2.485(8)
M–O[c] (Å)	2.384(2)	2.391(8)
M–O_w[d] (Å)	2.392(2)	2.358(9)
O–M–O[e](°)	66.38(7)	65.7(3)
O–M–O[f](°)	116.55(7)	119.2(3)
	118.08(7)	120.3(3)
	125.37(6)	120.4(3)
ϕ[g] (°)	0	0
	0	49.85(2)
	0	49.85(2)
M···M[h] (Å)	6.2447(3)	6.312(2)
	6.2531(3)	6.312(2)
	6.3948(3)	6.415(2)
M···M···M[i] (°)	103.908(4)	105.576(14)
	119.658(4)	124.522(15)
	131.273(4)	124.854(15)
V_0[j] (Å^3)	207 [22]	2036 [35]

[a]Value of the shape parameter relative to the ideal spherical version of the tricapped trigonal prismatic (TCTPR) and capped square antiprismatic (CSAPR) polyhedra. The corresponding value relative to the ideal Johnson version is given in parentheses (S = 0 for a perfect match with the considered polyhedron). [b]Average value of the equatorial metal-oxygen bond lengths of the TCTPR polyhedron from oxalates. [c]Average value of the basal metal-oxygen bond lengths of the TCTPR polyhedron from oxalates. [d]Average value of the basal metal-oxygen bond lengths of the TCTPR polyhedron from coordinated waters. [e]Average value of the bite metal-oxygen bond angles from oxalates. [f]Values of the equatorial metal-oxygen bond angles of the TCTPR polyhedron from oxalates [g]Values of the dihedral angle between the mean planes defined by the three metal ions from each pair of edge-sharing trinuclear unit around each of the three coordinated oxalate ion per Ho atom (see Fig. S4). [h]Values of the intralayer/intranet intermetallic distances across the oxalate bridges. [i]Values of the intralayer/intranet intermetallic angles across the oxalate bridges. [j]Value of the estimated solvent accessible void, calculated with the Platon Calc(full) routine after removing the crystallization water molecules from the structure (the percentage value relative to the total unit cell volume is given in brackets).

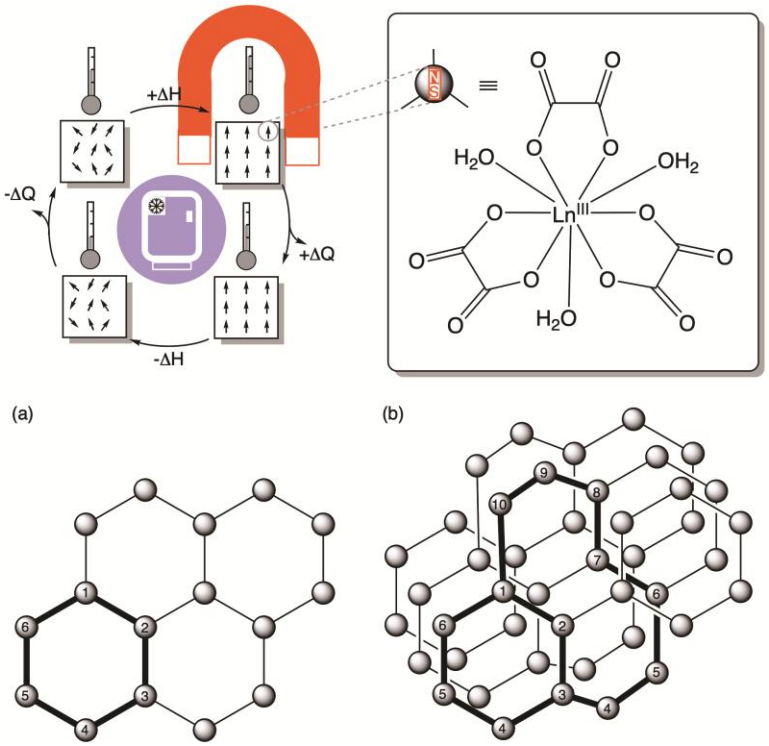

Scheme S1 Illustration of the MCE upon on/off switching of the applied magnetic field in 2D and 3D Ln MOFs based on the family of neutral lanthanide(III) sesquioxalate hydrates with hexagonal layer (a) or mixed hexagonal/decagonal net structures (b). The boxed structure shows the mononuclear triaquatris(oxalate)lanthanide(III) building units acting as tris(bidentate) tectons.

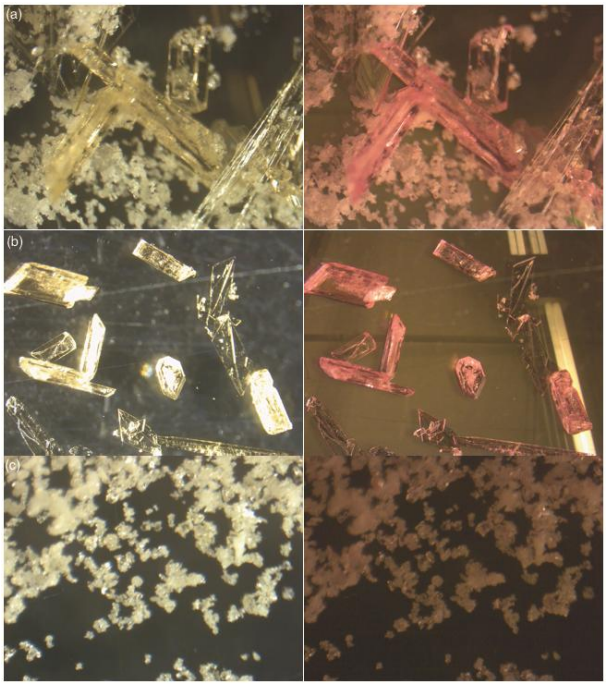

Fig. S1 Optical microscopy images under natural light (left) and fluorescent lamp (right) illumination corresponding to a mixture of single crystals of **1** and **2** (a) or pure crystals of **1** (b) and **2** (c) obtained by slow diffusion techniques at 25, 50, and 5 °C, respectively.

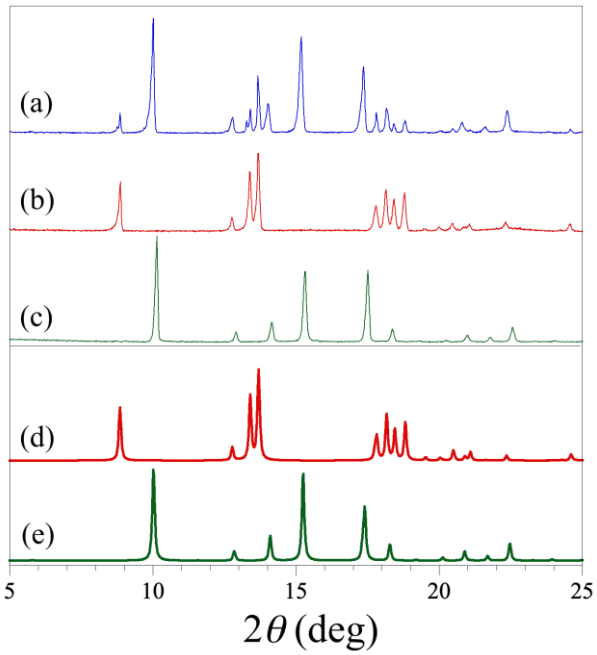

Fig. S2 Powder X-ray diffractograms corresponding to a mixture of single crystals of **1** and **2** (a) or pure crystals of **1** (b) and **2** (c) obtained by slow diffusion techniques at 25, 50, and 5 °C, respectively. The calculated diffractograms from the single-crystal XRD of **1** (d) and **2** (e) are shown for comparison.

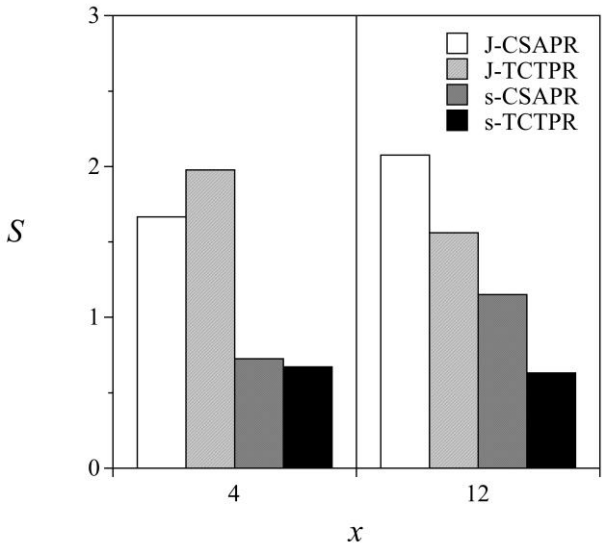

Fig. S3 Variation of the shape parameter (*S*) for the Johnson (J) and spherical (s) versions of the tricapped trigonal prism (TCTPR) and the monocapped square antiprism (CSAPR) with the number of crystallization water molecules (*x*) for **1** and **2** (data from Table S4).

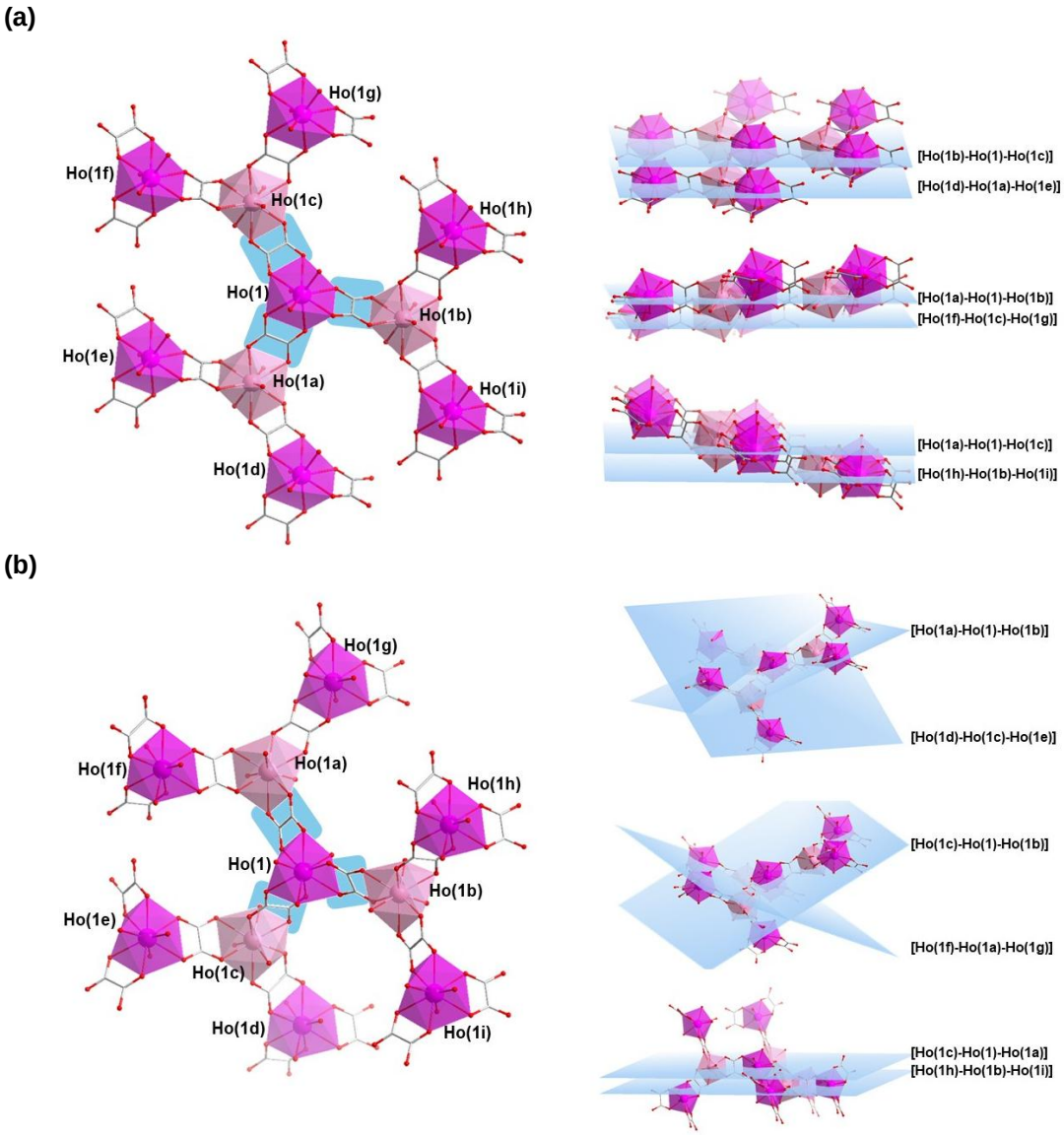

Fig. S4 A view of the first and second coordination sphere of the Ho(1) ion in both **1** (a) and **2** (b), with the metal atom numbering scheme (left), showing the relative orientation of the mean planes of the three pairs of edge-sharing trinuclear entities around the three oxalate bridges (right). The mononuclear units of opposite chirality are shown as dark and light purple polyhedra [Symmetry codes for **1**: (a) -*x*+1, -*y*+1, -*z*+1; (b) -*x*+2, -*y*+1, -*z*+1; (c) -*x*+1, -*y*+1, -*z*; (d) *x*-1, *y*, *z*; (e) *x*, *y*, *z*+1; (f) *x*+1, *y*, *z*+1; (g) *x*+1, *y*, *z*; (h) *x*, *y*, *z*-1; (i) *x*-1, *y*, *z*-1. Symmetry codes for **2**: (a) *x*-*y*+2/3, *x*+1/3, -*z*+4/3; (b) -*x*+1, -*y*+1, -*z*+2; (c) *y*-1/3, -*x*+*y*+1/3, -*z*+4/3; (d) -*y*+2/3, *x*-*y*+1/3, *z*-2/3; (e) -*x*+y, -*x*+1, *z*; (f) -*y*+1, *x*-*y*+1, *z*; (g) -*x*+*y*+2/3, -*x*+4/3, *z*-2/3; (h) -*y*+4/3, *x*-*y*+2/3, *z*+2/3; (i) -*x*+*y*+1/3, -*x*+2/3, *z*+2/3].

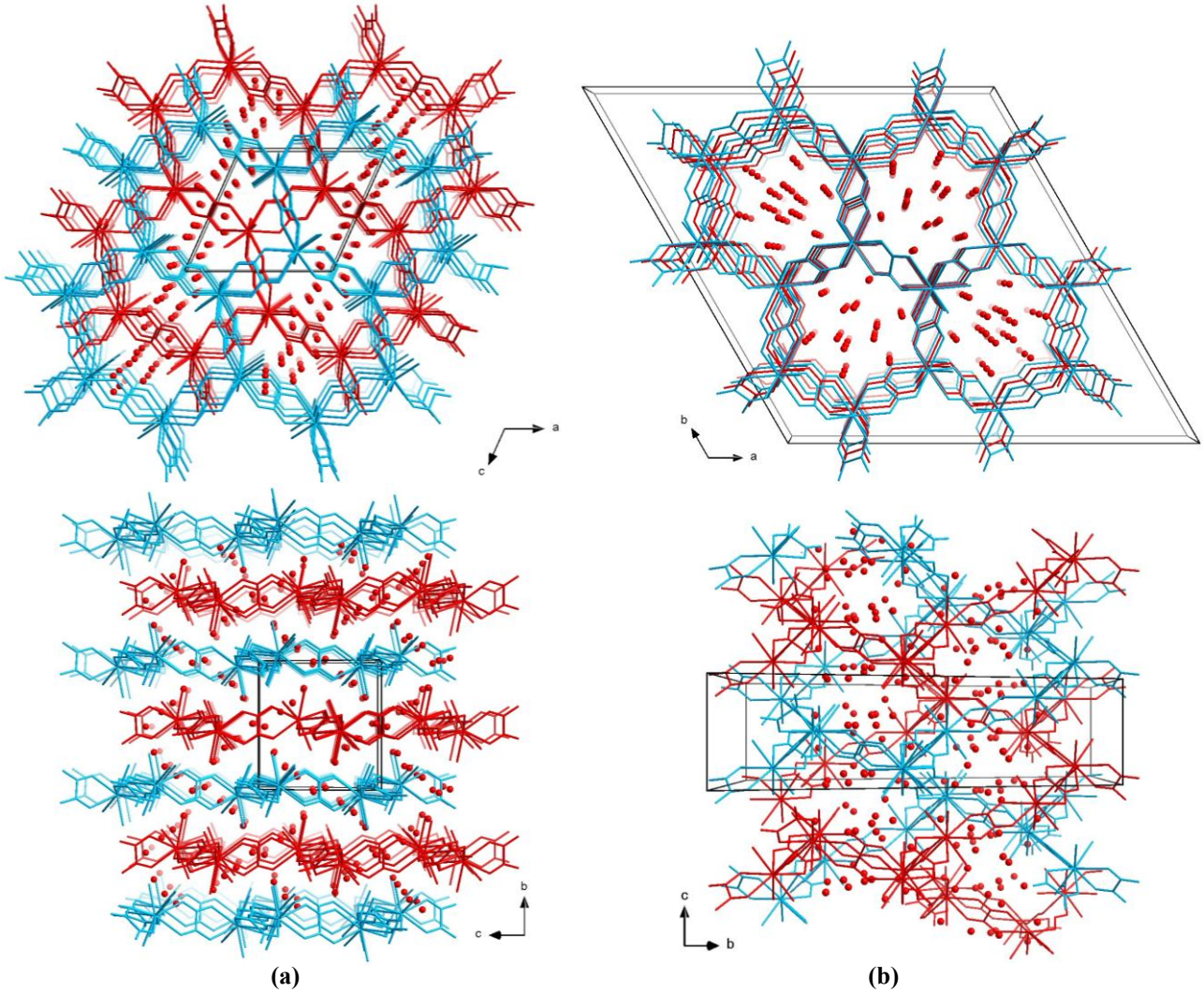

Fig. S5 Crystal packing views of **1** (a) and **2** (b) along the crystallographic *b* and *c* axes, respectively (top), and along the crystallographic *a* axis (bottom). The adjacent hexagonal layers (**1**) and interpenetrated mixed hexagonal/decagonal nets (**2**) are shown in different colors for clarity. The crystallization water molecules are represented by red spheres (all the disordered water sites are depicted for **1**). Hydrogen bonds are not shown for clarity.

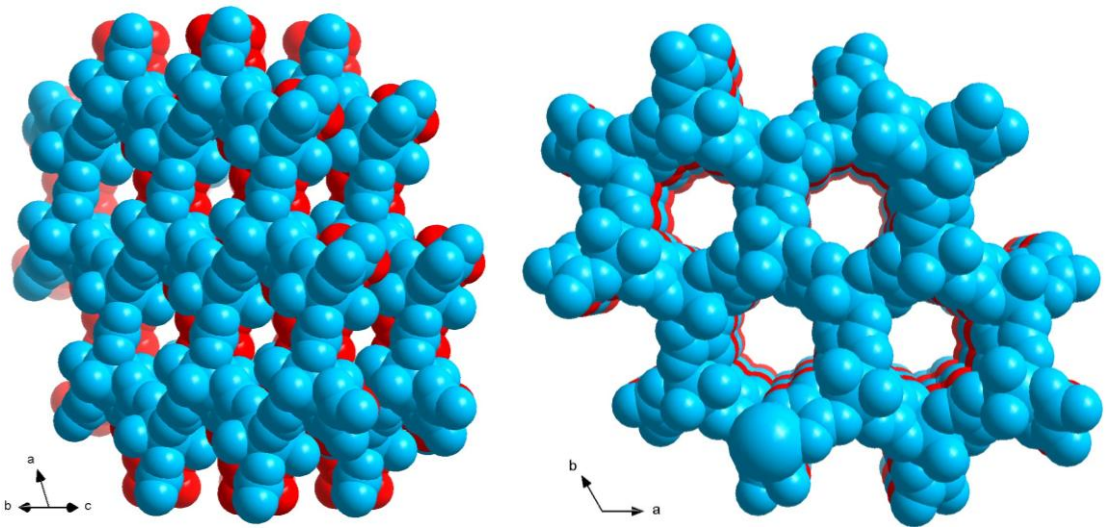

(a) **(b)**

Fig. S6 Space-filling model views of the crystal packing of **1** (a) and **2** (b) along the [011] and [001] directions, respectively, excluding the crystallization water molecules. The adjacent hexagonal layers (**1**) and interpenetrated mixed hexagonal/decagonal nets (**2**) are shown in different colors for clarity.

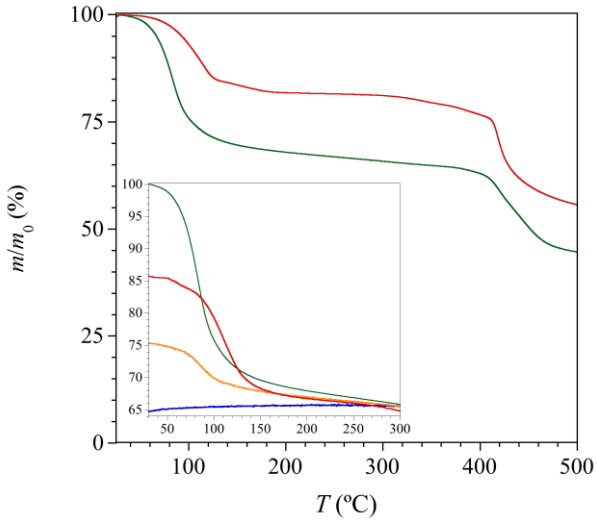

Fig. S7 TGA profiles of **1** (red line) and **2** (green line) under a dry N_2 atmosphere. The inset shows the TGA profiles corresponding to the dehydration/rehydration cycles after heating of **2** at 300 °C under a dry N_2 atmosphere (green line) to give **3** and subsequent exposition of **3** in the open air at room temperature for one day (blue line) or under water vapor saturated atmosphere for 3 days (orange line) or 3 weeks (red line) to render **1**.

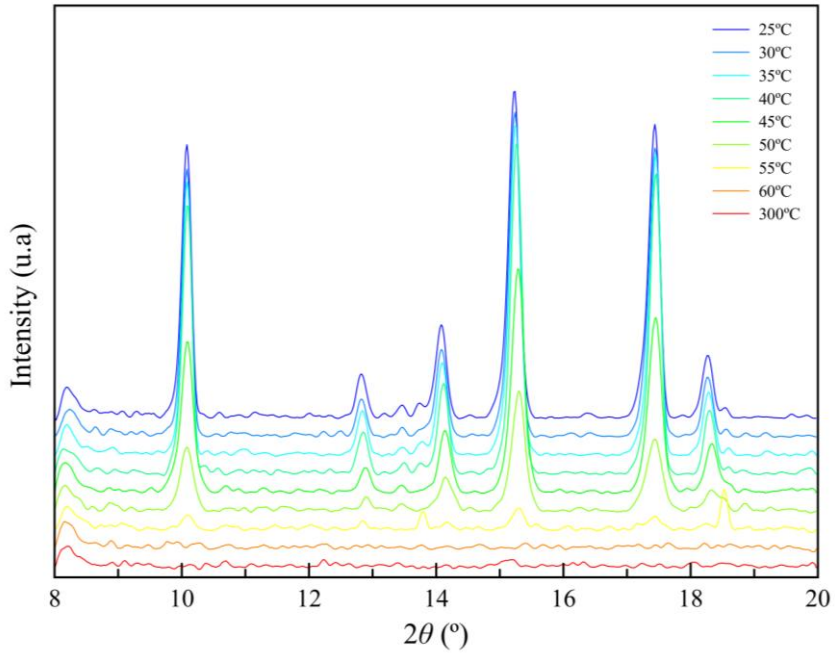

Fig. S8 Temperature dependence of the powder XRD pattern corresponding to the dehydration process after heating **2** from 25 to 300 ºC (from blue to red) to give **3**.

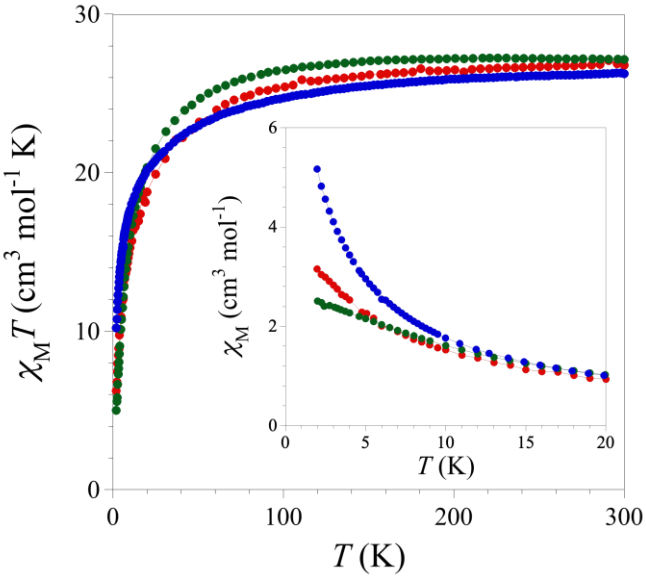

Fig. S9 Temperature dependence of $\chi_M T$ for **1** (●), **2** (●), and **3** (●) under applied *dc* fields of 0.025 ($T \leq 20$ K) and 5 T ($T > 20$ K). The inset shows the temperature dependence of χ_M in the low-temperature region. The solid lines are only eye-guides.

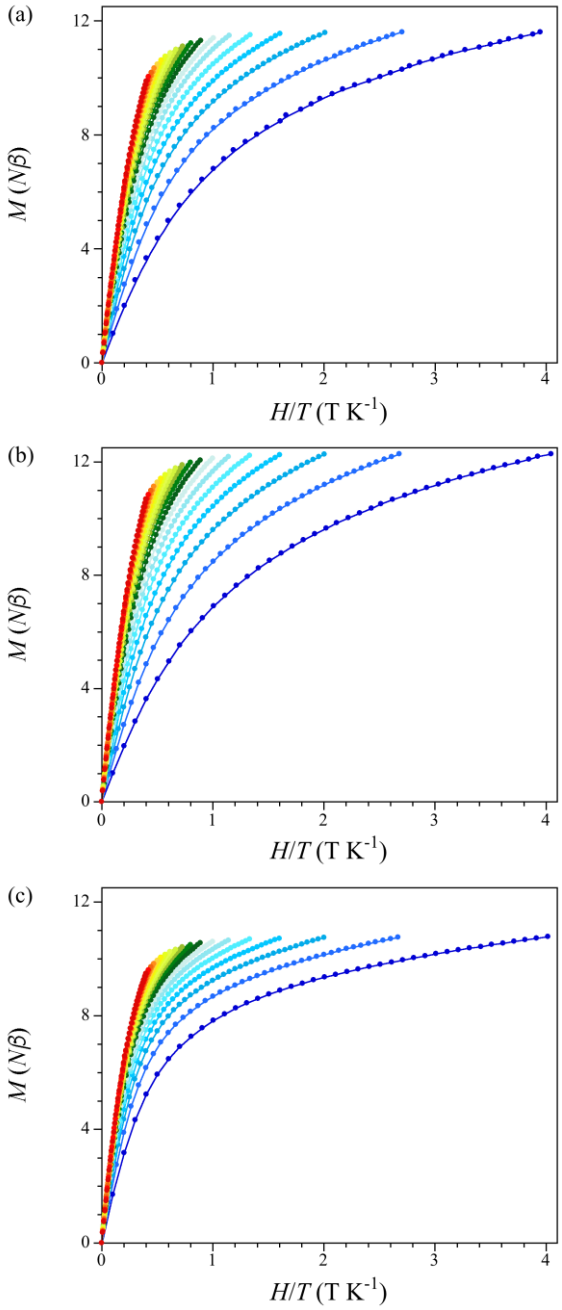

Fig. S10 Normalized field dependence of *M* for **1** (a), **2** (b), and **3** (c) in the temperature range 2–20 K (blue to red). The solid lines are only eye-guides.

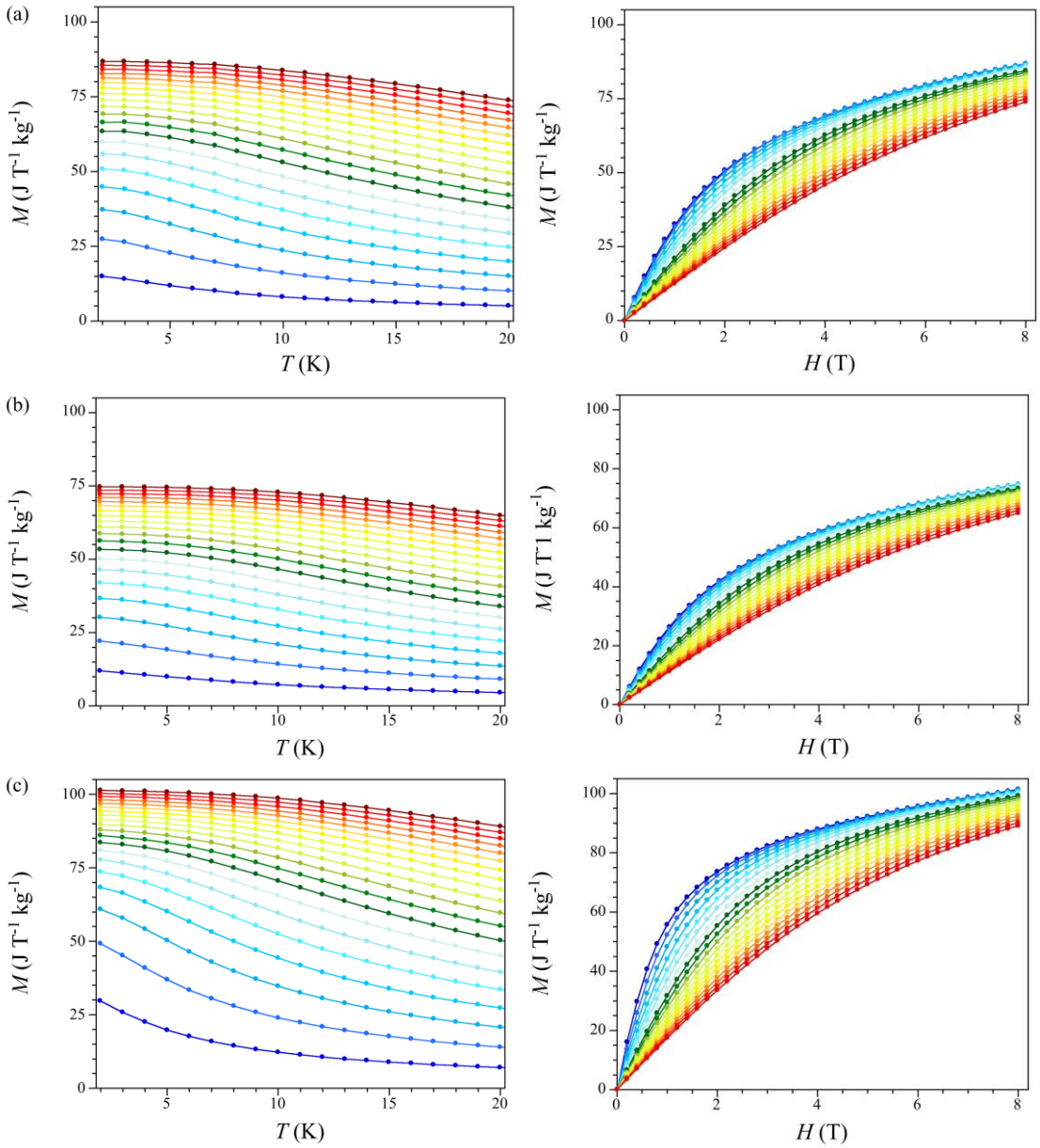

Fig. S11 Temperature (left) and field (right) dependence of *M* for **1** (a), **2** (b), and **3** (c) in the field change range 0–8 T and in the temperature range 2–20 K, respectively (blue to red). The solid lines are only eye-guides.

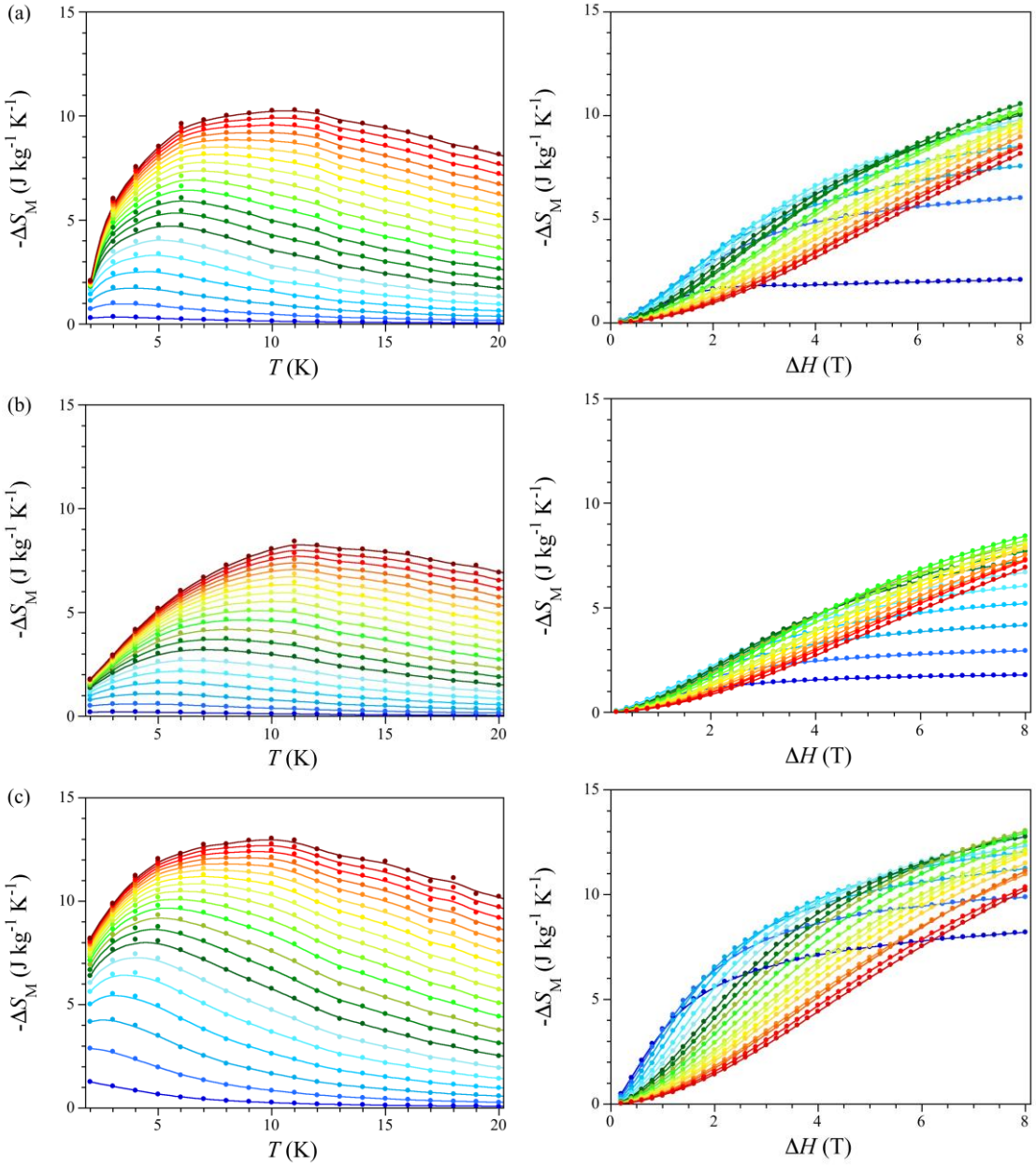

Fig. S12 Temperature (left) and field (right) dependence of $-\Delta S_M$ for **1** (a), **2** (b), and **3** (c) in the field change range 0–8 T and in the temperature range 2–20 K, respectively. The solid lines are only eye-guides.

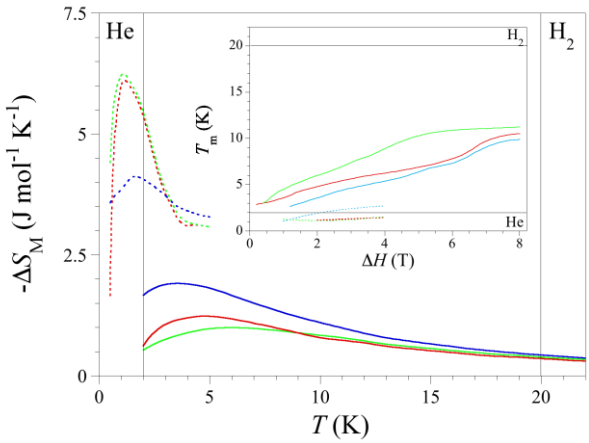

Fig. S13 Temperature dependence of $-\Delta S_M$ (per mol of lanthanide atom) for **1** (—), **2** (—), and **3** (—) compared to the gadolinium gallium garnet and its dysprosium-substituted derivatives GGG (---), DGGG (---), and DGG (---) at 2 T (data from ref. [9d]). The inset shows the magnetic field dependence for the temperature values of the $-\Delta S_M$ maxima (T_m). The He and H_2 liquefaction temperatures are outlined by black vertical or horizontal lines.